Hindawi
International Journal of Antennas and Propagation
Volume 2020, Article ID 7101752, 9 pages
https://doi.org/10.1155/2020/7101752

Research Article

Periodic Microstrip Leaky Wave Antenna with Double-Sided Shorting Pins and Pairs of Slots

Yahuan Chen, Kuang Wang, Yuanxin Li, and Yunliang Long

School of Electronics and Information Technology, Sun Yat-sen University, Guangzhou 510006, China

Correspondence should be addressed to Yuanxin Li; liyuanx@mail.sysu.edu.cn

Received 18 July 2020; Revised 10 September 2020; Accepted 17 September 2020; Published 30 September 2020

Academic Editor: Xiulong Bao

A backward to forward scanning periodic microstrip leaky wave antenna (MLWA) is presented. The proposed antenna consists of a long rectangular patch with alternating shorting pin on each side, which connects the antenna patch and the ground plane to form periodic shorting circuits. There are two pairs of slots alternately spaced on the long patch to suppress the open stop band (OSB). The OSB problem was initially reduced by optimizing the structural parameters, and the slotting on the patch further improved it. The measured radiation pattern in the *y*-*z* plane shows that the antenna can scan electronically from 142° to 39° toward the end-fire (+*z* direction) when the operating frequency changes from 6 GHz to 12.9 GHz. The measured gain is greater than 5 dBi over the entire operating band.

1. Introduction

Forward scanning microstrip leaky wave antenna (MLWA) first appeared in 1979 [1]. For more applications, microstrip periodic leaky wave antenna with forward and backward beam scanning capability was developed later [2].

A periodic MWLA is one in which there are multiple identical unit cells cascading along the propagation direction. The periodic structure is mainly composed of the following types of elements: strips (metallic strip [3], offset double-side parallel-strip line [4], and microstrip line [5]), stubs (open-ended stubs [6]), composite right/left handed [7], and slots [8]. However, periodic MLWAs have severe OSB problem at broadside. Various methods have been proposed to improve or eliminate OSB, including match the impedance within the unit cell [9, 10], employing asymmetry [11], and using two similar but nonidentical elements per unit cell [12]. OSB can also be inhibited by optimizing structural parameters, such as optimizing the diameter of the cylindrical holes in the dielectric image line [13] and varying the groove width of the spoof plasmons cells [14]. There are also some techniques to achieve broadside direction scanning, such as loading field-block structures [15–18].

Early years, a periodic half-width MLWA with backward to forward beam scanning capability is proposed in [19]. Then, in [20], a half-width MLWA with the periodic short circuits is developed, which has a feature of narrower antenna width. However, the configuration of these antenna designs has cost a lot of shorting pins, leading to a low radiation efficiency and small gain since the reduction of effective radiation boundary. At the same time, they have poor broadside radiation.

In this paper, a periodic MLWA, composed of a uniform rectangle microstrip patch leaky wave antenna with shorting pins periodically alternately loaded on its side, is presented. The configuration of the antenna is shown in Figure 1. Slotting method is introduced for OSB suppression, because the slots in the patch can reduce mutual coupling between adjacent cells [21]. Figure 2 shows the specific location of the slots in each unit cell. The last shorting pin in the right unit is canceled for connecting the load port on the end of the antenna. A broadband matching is introduced for a better *S*-parameter through the overall bandwidth. Simulated and measured results of far-field radiation patterns, *S*-parameters, and gain are displaced.

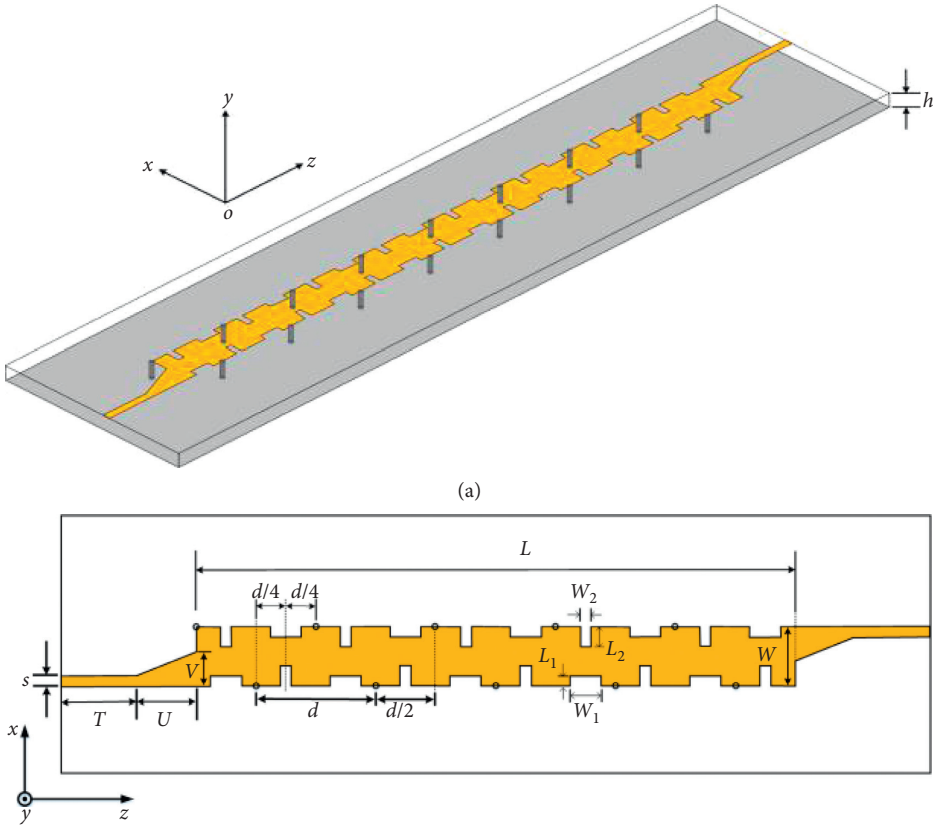

Figure 1: The proposed periodic microstrip leaky wave antenna with double-sided shorting pins. (a) 3D view. (b) Top view.

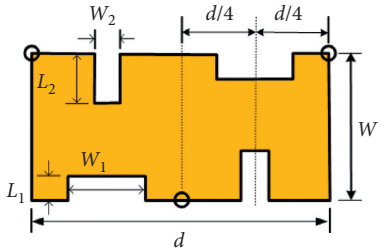

Figure 2: Schematic diagram of the periodic unit structure with length d.

2. Design Description

As an important improved design of [19, 20], the proposed antenna proves that only a single shorting pin can form a periodic structure to achieve backward to forward beam scanning, instead of a series. In each periodic unit of length d, the distance between short-circuit pins on the same side of the patch is d, and the distance between short-circuit pins on different sides on the z-axis is $d/2$.

2.1. The Propagation Constant Achieved by Macrocell Method. MLWA have the beam scanning capacity with a change in operating frequency, which is controlled by the complex propagation constants k_{zn}. The complex propagation

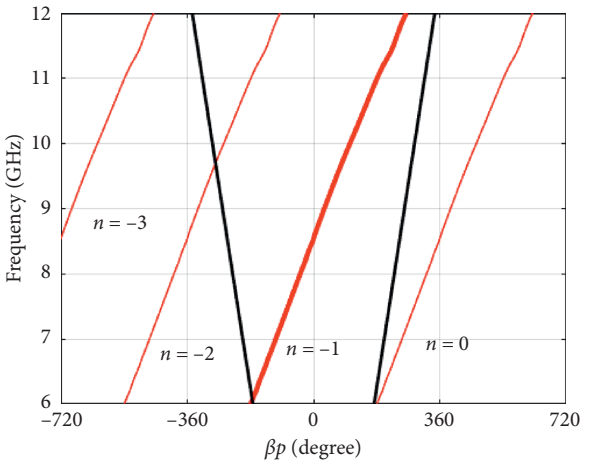

Figure 3: The dispersion diagram of proposed antenna.

constant k_{zn} of the periodic MLWAs is given by Floquet's theorem:

$$k_{zn} = \beta_{2zn} - j\alpha_{zn} = k_z + \frac{2n\pi}{p}, \quad n = \pm 1, \pm 2, \ldots, \tag{1}$$

where n is the order of the space harmonics (usually $n = -1$) and p is the period.

The direction of main beam is determined by the phase constant as follows:

$$\theta = \frac{\pi}{2} - \arcsin\left(\frac{\beta_{zn}}{k_0}\right), \tag{2}$$

where θ is the direction of the main beam and k_0 is the wavenumber of the free space.

The attenuation constant α_{zn} is a parameter that indicates the amplitude or power attenuation of an electromagnetic or electrical signal during transmission. It is mainly related to the main beam and can be given by

$$\frac{\alpha_{zn}}{k_0} = 0.18\theta_{HPBW}\cos\left(\frac{\pi}{2} - \theta\right), \tag{3}$$

where θ_{HPBW} is the half-power beam-width of the main beam. Through these formulas, the radiation performance of the antenna can be known from the propagation constant.

It can be known from the dispersion diagram that the working mode of the proposed antenna is the first high-order mode. The periodic MLWA can scan from the backward ($-z$ direction) to the forward ($+z$ direction) because the β_{-1} can vary from negative values to positive values in Figure 3.

The periodic structure can be seen as an infinite cascade of identical two-port networks [22], as shown in Figure 4. Each unit cell is characterized by the transmission matrix T:

$$\begin{pmatrix} V_{n+1} \\ I_{n+1} \end{pmatrix} = T\begin{pmatrix} V_n \\ I_n \end{pmatrix}. \tag{4}$$

The propagation of a Bloch mode with wavenumber $k_z = \beta_z - j\alpha_z$ corresponds to the condition:

$$\begin{pmatrix} V_{n+1} \\ I_{n+1} \end{pmatrix} = e^{-jk_z p}\begin{bmatrix} V_n \\ I_n \end{bmatrix}, \tag{5}$$

which shows that $e^{-jk_z p}$ is an eigenvalue of the matrix T.

However, the characterization of a single cell will neglect mutual coupling between adjacent cells. Then, an integer number of unit cells, namely, macrocell, are introduced. An N-macrocell is modeled through the matrix T_N, which can be calculated through the S-parameters by the conversion formulas. The S-parameters can be obtained by simulated or measured. The wavenumber $k_{z,i}$ can be given as [23]

$$\begin{aligned} k_{z,i} &= \frac{j}{N_p}\ln\left(\lambda_{N,i}\right), \\ &= -\frac{\mathrm{Arg}\left(\lambda_{N,i}\right)}{N_p} - \frac{2\pi m}{N_p} + j\frac{\ln\left|\lambda_{N,i}\right|}{N_p} = \beta_{z,i} - j\alpha_{z,i}, \end{aligned} \tag{6}$$

where $\lambda_{N,i}$ are eigenvalues of the matrix T_N, N_p is the distance between the ports of the network.

2.2. Structure Parameter Analysis. Figures 5 and 6 are the normalized phase and attenuation constants calculated by equation (4) using the simulated S-parameters. As shown in Figure 5, when the distance between the two shorting pins on the same side d is changed from 28 mm to 20 mm, the phase constant curve is shifted to a higher frequency. The influence of the width of the antenna W on the phase constant is displayed in Figure 6. As W decreases from 13 mm to 7 mm, the phase constant curve moves to higher frequencies.

This means the operating band shifts to a lower frequency band as d increases, and the increase in W causes a similar consequence.

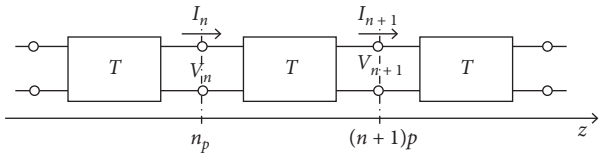

Figure 4: Equivalent network of a periodic line with minimal period p.

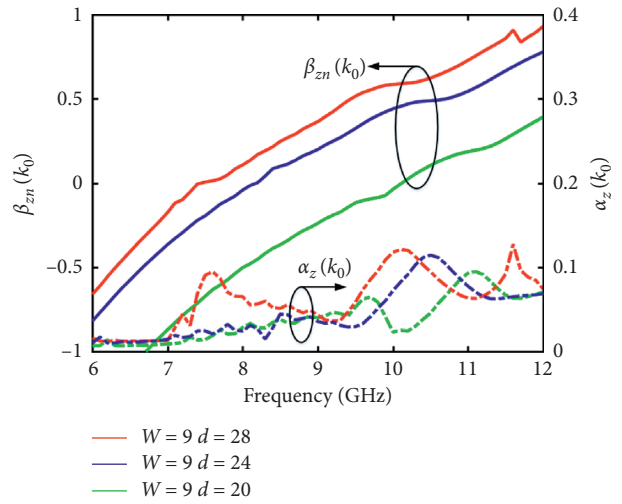

Figure 5: The normalized propagation wavenumbers of the proposed periodic antenna with different d ($W = 9$ mm).

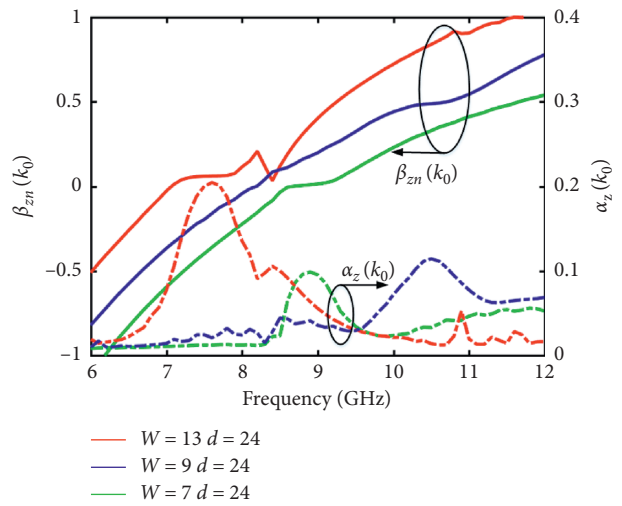

Figure 6: The normalized propagation wavenumbers of the proposed periodic antenna with different W ($d = 24$ mm).

In the process of changing the structural parameters, it was found that the OSB in this structure is related to the ratio of d/W. The OSB could be suppressed when the appropriate parameters are selected. Figure 7–11 are the plot of propagation constants when $d/W = 1$, $d/W = 1.5$, $d/W = 2$, $d/W = 2.5$, and $d/W = 3$, respectively. It can be seen that the scanning performance at broadside direction varies with different d/W. And when d/W is consistent, the antenna composed of different d and W have similar performances in the vicinity of the OSB band.

Therefore, a preliminary law that can effectively suppress OSB is obtained based on the simulation research. According to the ratio d/W, this structure can be divided into the following categories.

If $d/W \leq 1$, the proposed antenna can only perform forward scanning because it is too dense to form a periodic structure, as shown in Figure 7.

Else if $1 < d/W \leq 2$, the proposed antenna can scan forward and backward but has obvious OSB, as shown in Figures 8 and 9.

Else if $d/W > 2$, the OSB will disappear, as shown in Figure 10.

However, the d/W range where the OSB does not exist is very small. The OSB will reappear when the ratio expanded further, as shown in Figure 11.

2.3. OSB Optimization. The main manifestation of OSB is the serious degradation of the pattern when scanning through the broadside, and what shown in the phase constant curve is a stagnation around $\beta = 0$ and a sudden increase in the attenuation constant.

In order to further suppress the OSB, we etch two pairs of slots on the metal patch. The alternately spaced pairs of slot on the patch can change the impedance of the unit cell. After adjusting the width and length of each pair of the slot, the unit cells have been well matched. It may be diminished or suppressed by introducing two radiating elements in the periodic unit, or by adjusting the structural parameters to optimize the distance between the component pairs.

Figure 12(a) and 12(b) are the electric field distribution of the proposed antenna without slots when the phase is 0 and 90 degrees, respectively. Figure 12(c) and 12(d) are the electric field distribution of the proposed antenna with slots when the phase is 0 and 90 degrees, respectively. It can be seen that both phases of the un-slotted antenna at the OSB frequency point show a significant standing wave behavior, that is, a nearly vertical zero potential. After slotting, the zero potential is no longer vertical, but a form of propagation. The almost standing wave behaviors are improved after etched pairs of slots on the patch, which means the performance of the MLWA around broadside have been better.

Figure 13 is the normalized phase constants and S-parameter simulated by *HFSS*. It shows that the phase constant and S-parameter of the antenna will change when the dimensions of the slots on the patch change. By comparing the red and blue curves, it can be seen that, as L_1 increases, the OSB becomes serious and the phase constant curve moves slightly upward. The increase of L_2 also leads to the same

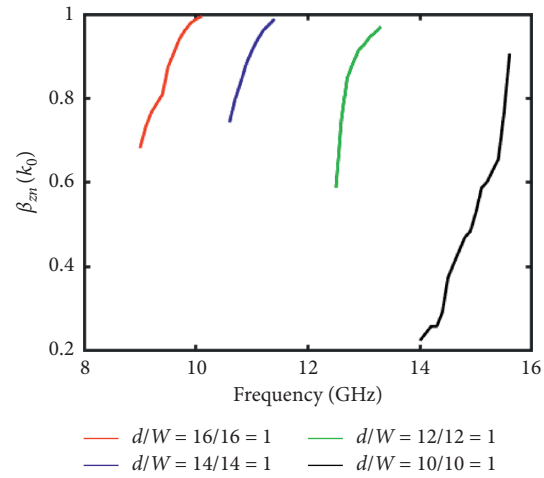

Figure 7: The normalized propagation constant of different parameters when $d/W = 1$.

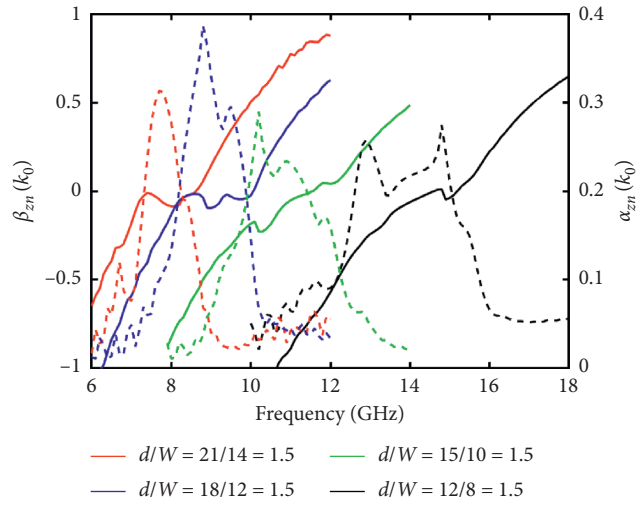

Figure 8: The normalized propagation constant of different parameters when $d/W = 1.5$.

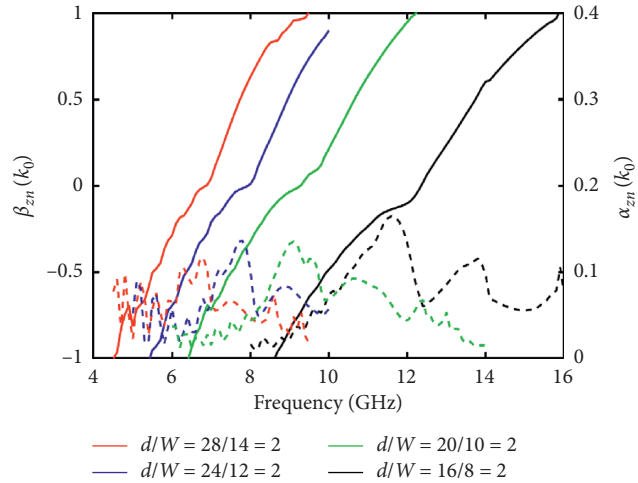

Figure 9: The normalized propagation constant of different parameters when $d/W = 2$.

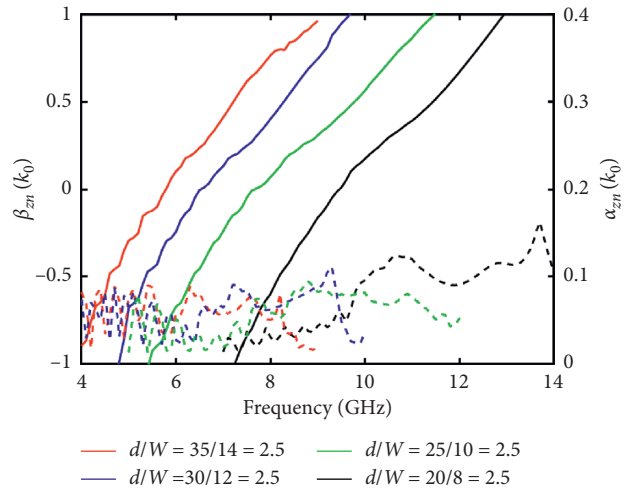

Figure 10: The normalized propagation constant of different parameters when $d/W = 2.5$.

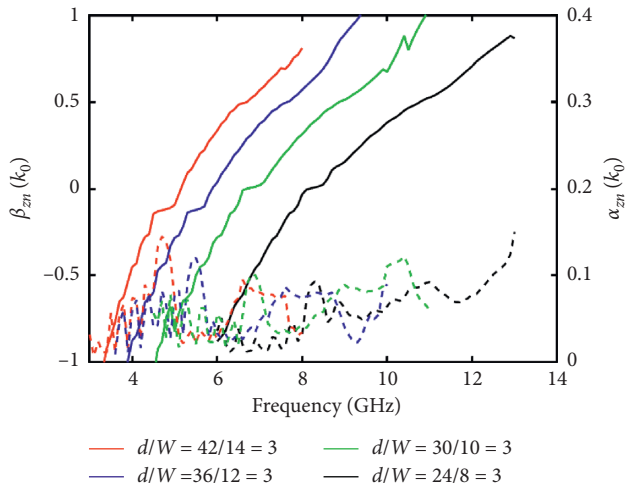

Figure 11: The normalized propagation constant of different parameters when d/$W = 3$.

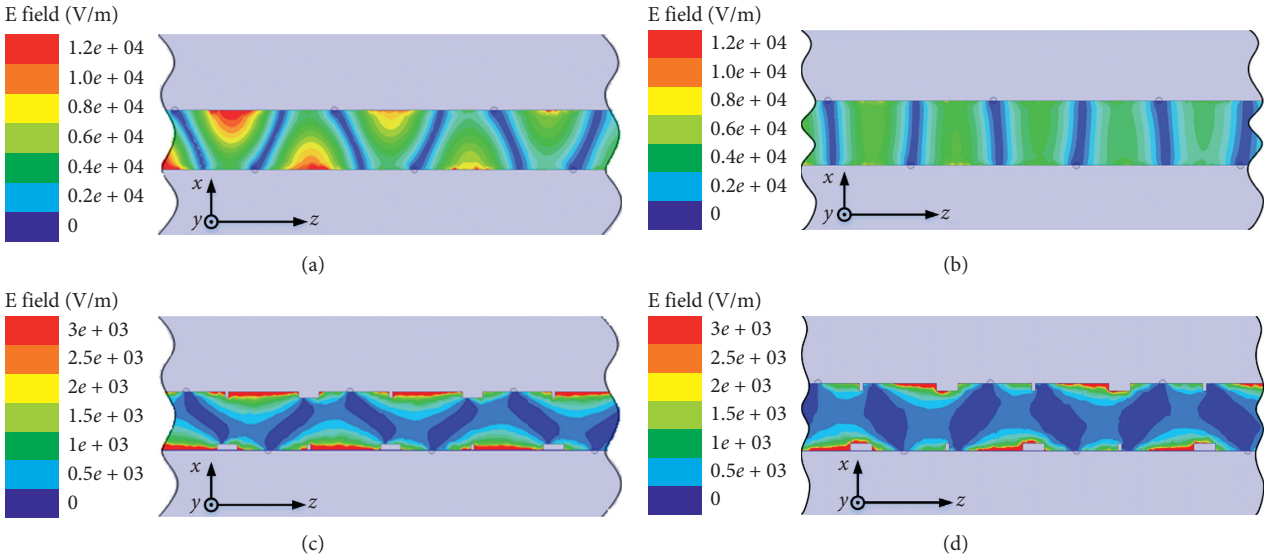

Figure 12: Electric field distribution of the proposed antenna at OSB frequency. (a) Without slots, phase = 0 degree. (b) Without slots, phase = 90 degree. (c) With slots, phase = 0 degree. (d) With slots, phase = 90 degree.

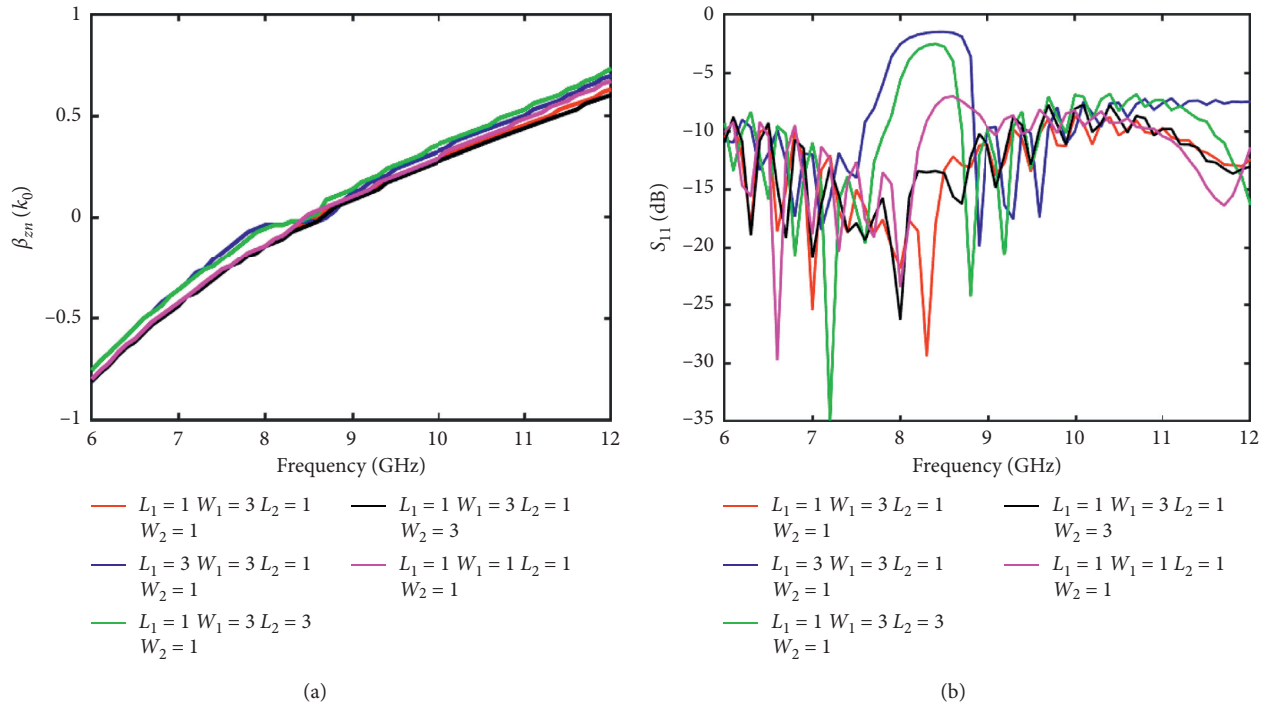

Figure 13: The simulated normalized phase constants and S-parameters of the proposed periodic antenna with different slot parameters.

results between the red the green curves. According to the red and black curve, the phase constant curve is unchanged as W_2 increases, but the OSB becomes more obvious. The same result can be obtained for the parameter $W1$ by comparing the red and magenta curves. In other words, the length of the slot has an effect on the phase curve, and the width of the slot can only affect the S-parameter. So, the performance of antenna can be optimized through varying the slot dimension.

Figure 14 is the comparison of propagation constant of proposed antenna with and without slots. The antenna with slots has a smaller attenuation constant than the antenna without slots, especially near the OSB (around 8.3 GHz). This shows that the slot on the antenna patch can indeed suppress the OSB.

3. Antenna Structure

Figure 15(a) is a prototype of the proposed antenna, which is printed on a dielectric slab (relative dielectric constant $\varepsilon r = 2.45$ and dielectric loss tangent $\tan \delta = 0.005$). The radius of each of these pins is 0.5 mm. Figure 15(b) shows the details of the pins and slots in the prototype antenna. Other values of parameters are listed in Table 1.

4. Measurement Results

The far-field radiation pattern of the proposed periodic MLWA in the $y-z$ plane is measured. As described above, the antenna scans from $-z$ direction to the $+z$ direction through broadside with frequency increase.

Figure 16 shows the measured and simulated normalized phase constants and attenuation constants. The

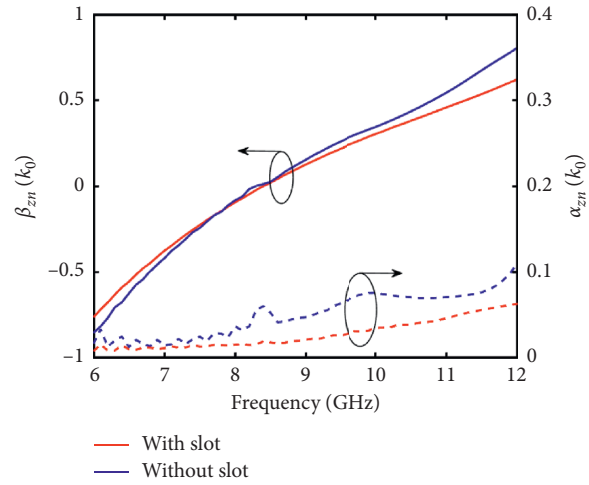

Figure 14: The comparison of propagation constant of proposed antenna with and without slots.

measurement results are in good agreement with the simulation results. The phase constant curve varies smoothly and no OSB appears near the zero point of the curve.

Figure 17 shows the measured pattern of backward quadrant and are pointed to $\theta = 137^\circ$, $\theta = 125^\circ$, and $\theta = 115^\circ$ at 6.2 GHz, 6.6 GHz, and 7 GHz, respectively. It can be seen from Figure 18 that the antenna can radiate through the broadside direction, i.e, $\theta = 100^\circ$ at 7.8 GHz, $\theta = 90^\circ$ at 8.6 GHz, and $\theta = 80^\circ$ at 9.4 GHz. When the operating frequency changes from 10.4 GHz to 12 GHz, the main beams scan from $\theta = 70^\circ$ to $\theta = 51^\circ$ in the forward quadrant, as displayed in Figure 19. Experimental results show that, as the operating frequency increases from 6 GHz to 12.9 GHz, the

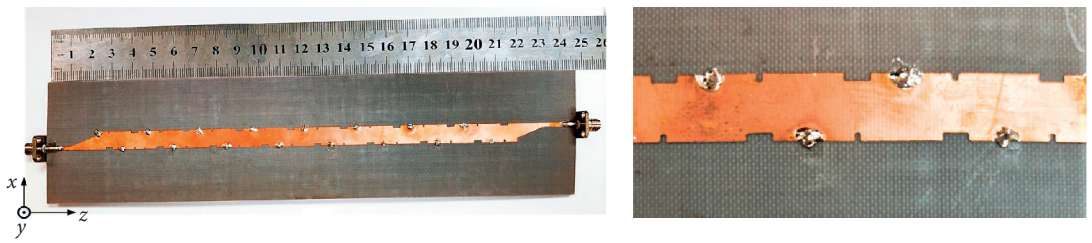

(a) (b)

Figure 15: (a) Prototype of the proposed periodic MLWA with double-sided shorting pins. (b) Details of the pins and slots in the proposed antenna.

Table 1: Dimensions of the proposed periodic MLWA.

Parameters	Values (mm)	Parameters	Values (mm)	Parameters	Values (mm)
d	24	S	2.2	W_1	3
W	9	T	15	L_1	1
L	192	V	7	W_2	1
h	0.8	U	12	L_2	1

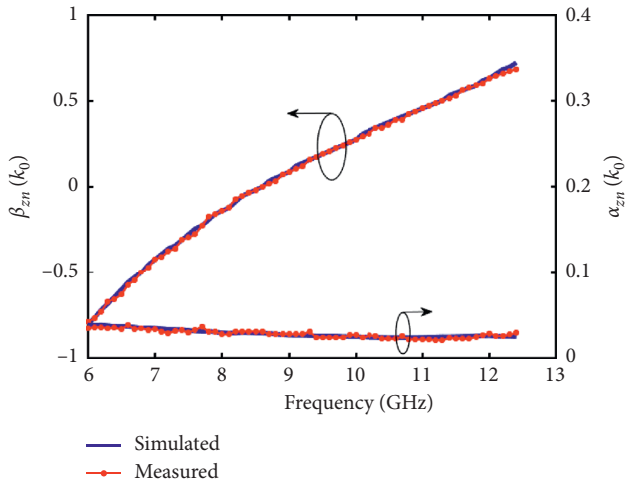

Figure 16: The measured and *HFSS* simulated normalized propagation constants of the proposed periodic MLWA.

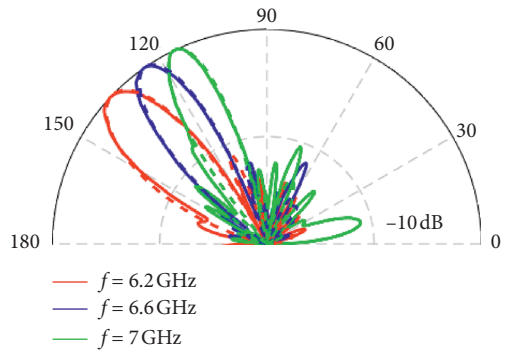

Figure 17: The measured radiation pattern of the proposed periodic MLWA in the backward (—— measured ---- simulated).

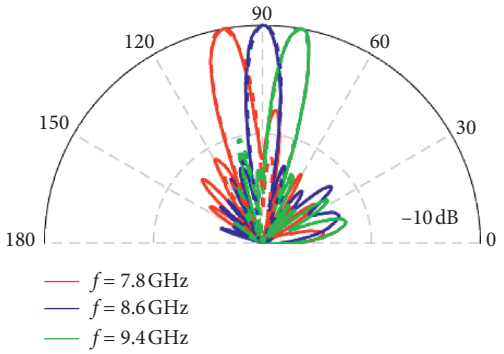

Figure 18: The measured radiation pattern of the proposed periodic MLWA at the broadside (—— measured ---- simulated).

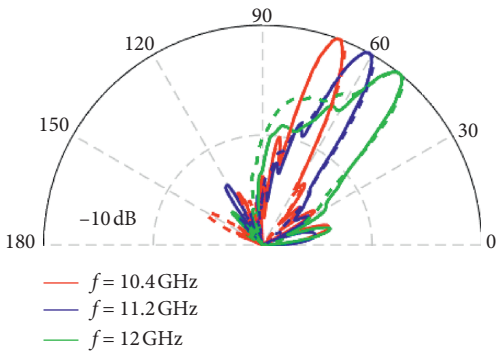

Figure 19: The measured radiation pattern of the proposed periodic MLWA in the forward (—— measured ---- simulated).

main beam of the proposed antenna electronically and continuously scans from $\theta = 142^\circ$ to $\theta = 39^\circ$ in the y–z plane. The antenna performs well when scanning from backward to forward, even though the scanning beam passes through the broadside. The OSB has been suppressed.

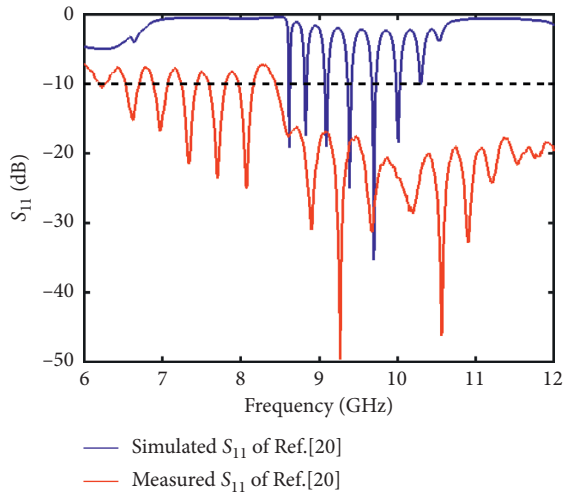

Figure 20: The *S*-parameter of the antenna of [20] and the proposed periodic MLWA antenna.

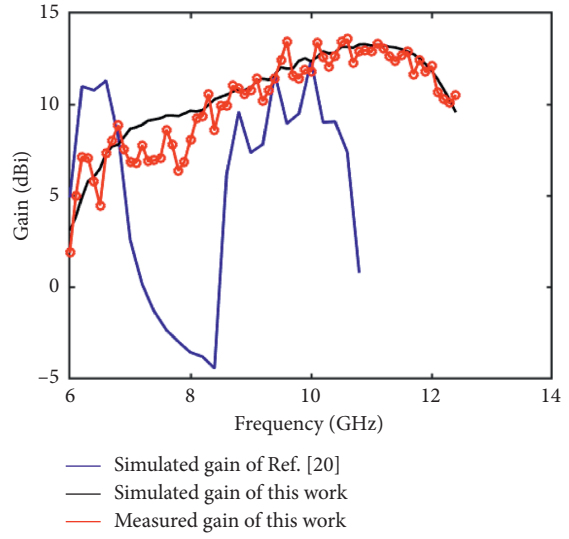

Figure 21: The gain of the antenna of [20] and the proposed periodic MLWA antenna.

Table 2: Comparison of the proposed antenna with previous antenna design.

Ref.	Frequency (GHz)	Scan range (deg)	Gain (dBi)	OSB band (GHz)	Pins' number
This work	6~12.9	142~39	5~13.6	None	16
[17]	4.2~8.9	149~28	—	5.4~6.1	80
[18]	4.4~8.8	144~41	1~9	5.3~6.2	71

Figures 20 and 21 are the comparison of the *S*-parameters and gain between the proposed antenna and the antenna of [20]. It can be seen that the antenna in [20] has obvious OSB and regardless of radiation pattern or gain, and the OSB is basically invisible in the proposed antenna. The *S*-parameter of the forward scanning band of the proposed antenna is better than that of the backward. The gain of the proposed antenna is above 5 dBi when the operation frequency is higher than 6 GHz. Regardless of radiation pattern or gain, the OSB is basically invisible in the measurement results.

The comparison between the proposed antenna and previous work is shown in Table 2. The gain of the proposed antenna is greater than that of previous work. More importantly, the OSB in the antenna is nearly suppressed. The number of the pins was substantially reduced which resulted in a compact structure.

5. Conclusion

In this study, an improved MLWA with reduced shorting pins is submitted. The proposed antenna consists of shorting pins periodically loaded on both sides of the long rectangular patch, and the distance of each shorting pin on the z-axis is $d/2$. In order to suppress OSB, two pairs of slots are introduced in each unit. Experimental results show that, as the operating frequency increases from 6 GHz to 12.9 GHz, the main beam of the proposed antenna electronically and continuously scans from $\theta = 142^{\circ}$ to $\theta = 39^{\circ}$ in the y-z plane. This antenna design is simple, easy to manufacture, and can be useful in vehicle radar systems.

Data Availability

The data used to support the findings of this study are available from the corresponding author upon request.

Conflicts of Interest

The authors declare that they have no conflicts of interest.

Acknowledgments

This work was supported in part by the Natural Science Foundation of China under Grants 61971453 and 61701549 and Nature Science Foundation of Guangdong Province under Grants 2015A030312010.

References

[1] W. Menzel, "A new travelling-wave antenna in microstrip," in *Proceedings of 8th European Microwave Conference*, vol. 33, no. 4, pp. 137–140, Paris, France, September 1978.

[2] D. R. Jackson, A. A. Oliner, and C. A. Balanis, *Leaky-Wave Antennas in Modern Antenna Handbook*, Wiley, Hoboken, NJ, USA, 2008.

[3] M. Wang, H. F. Ma, H. C. Zhang, W. X. Tang, X. R. Zhang, and T. J. Cui, "Frequency-fixed beam-scanning leaky-wave antenna using electronically controllable corrugated microstrip line," *IEEE Transactions on Antennas and Propagation*, vol. 66, no. 9, pp. 4449–4457, 2018.

[4] D. Ye, Y. Li, Z. Liang, J. Liu, S. Zheng, and Y. Long, "Periodic triangle-truncated DSPSL-based antenna with backfire to endfire beam-scanning capacity," *IEEE Transactions on Antennas and Propagation*, vol. 65, no. 2, pp. 845–849, Feb. 2017.

[5] M. H. Rahmani and D. Deslandes, "Backward to forward scanning periodic leaky-wave antenna with wide scanning range," *IEEE Transactions on Antennas and Propagation*, vol. 65, no. 7, pp. 3326–3335, 2017.

[6] Y.-L. Lyu, F.-Y. Meng, G.-H. Yang, P.-Y. Wang, Q. Wu, and K. Wu, "Periodic leaky-wave antenna based on complementary pair of radiation elements," *IEEE Transactions on Antennas and Propagation*, vol. 66, no. 9, pp. 4503–4515, 2018.

[7] H. Lee, J. H. Choi, C.-T. M. Wu, and T. Itoh, "A compact single radiator CRLH-inspired circularly polarized leaky-wave antenna based on substrate-integrated waveguide," *IEEE Transactions on Antennas and Propagation*, vol. 63, no. 10, pp. 4566–4572, 2015.

[8] R. Henry and M. Okoniewski, "A broadside scanning substrate integrated waveguide periodic phase-reversal leaky-wave antenna," *IEEE Antennas and Wireless Propagation Letters*, vol. 15, pp. 602–605, 2016.

[9] J. T. Williams, P. Baccarelli, S. Paulotto, and D. R. Jackson, "1-D combline leaky-wave antenna with the open-stopband suppressed: design considerations and comparisons with measurements," *IEEE Transactions on Antennas and Propagation*, vol. 61, no. 9, pp. 4484–4492, 2013.

[10] D. K. Karmokar, Y. J. Guo, P.-Y. Qin, S.-L. Chen, and T. S. Bird, "Substrate integrated waveguide-based periodic backward-to-forward scanning leaky-wave antenna with low cross-polarization," *IEEE Transactions on Antennas and Propagation*, vol. 66, no. 8, pp. 3846–3856, 2018.

[11] S. Otto, Z. Chen, A. Al-Bassam, A. Rennings, K. Solbach, and C. Caloz, "Circular polarization of periodic leaky-wave antennas with axial asymmetry: theoretical proof and experimental demonstration," *IEEE Transactions on Antennas and Propagation*, vol. 62, no. 4, pp. 1817–1829, 2014.

[12] J. Liu, W. Zhou, and Y. Long, "A simple technique for open-stopband suppression in periodic leaky-wave antennas using two nonidentical elements per unit cell," *IEEE Transactions on Antennas and Propagation*, vol. 66, no. 6, pp. 2741–2751, 2018.

[13] C. S. Prasad and A. Biswas, "Dielectric image line-based leaky-wave antenna for wide range of beam scanning through broadside," *IEEE Transactions on Antennas and Propagation*, vol. 65, no. 8, pp. 4311–4315, 2017.

[14] A. Kianinejad, Z. N. Chen, and C.-W. Qiu, "A single-layered spoof-plasmon-mode leaky wave antenna with consistent gain," *IEEE Transactions on Antennas and Propagation*, vol. 65, no. 2, pp. 681–687, 2017.

[15] L. Chang, Y. Li, Z. Zhang, S. Wang, and Z. Feng, "Planar air-filled terahertz antenna array based on channelized coplanar waveguide using hierarchical silicon bulk micromachining," *IEEE Transactions on Antennas and Propagation*, vol. 66, no. 10, pp. 5318–5325, 2018.

[16] L. Chang, Z. Zhang, Y. Li, and M. F. Iskander, "Single-layer magnetic current antenna array with high realized aperture usage rate based on microstrip line structure," *IEEE Transactions on Antennas and Propagation*, vol. 65, no. 2, pp. 584–592, 2017.

[17] L. Chang, Y. Li, Z. Zhang, and Z. Feng, "Horizontally polarized omnidirectional antenna array using cascaded cavities," *IEEE Transactions on Antennas and Propagation*, vol. 64, no. 12, pp. 5454–5459, 2016.

[18] L. Chang, Z. Zhang, Y. Li, and Z. Feng, "Wideband triangular-cavity-cascaded antennas," *IEEE Transactions on Antennas and Propagation*, vol. 64, no. 7, pp. 2840–2847, 2016.

[19] Y. Li, Q. Xue, E. K. Yung, and Y. Long, "The periodic half-width microstrip leaky-wave antenna with a backward to forward scanning capability," *IEEE Transactions on Antennas and Propagation*, vol. 58, no. 3, pp. 963–966, 2010.

[20] Y. Li, Q. Xue, H.-Z. Tan, and Y. Long, "The half-width microstrip leaky wave antenna with the periodic short circuits," *IEEE Transactions on Antennas and Propagation*, vol. 59, no. 9, pp. 3421–3423, 2011.

[21] L. Liu, C. Liu, Z. Li, X. Yin, and Z. N. Chen, "Slit-slot line and its application to low cross-polarization slot antenna and mutual-coupling suppressed tripolarized MIMO antenna," *IEEE Transactions on Antennas and Propagation*, vol. 67, no. 1, pp. 4–15, Jan. 2019.

[22] D. M. Pozar, *Microwave Engineering*, Wiley, New York, NY, USA, 3rd edition, 2004.

[23] G. Valerio, S. Paulotto, P. Baccarelli, P. Burghignoli, and A. Galli, "Accurate bloch analysis of 1-D periodic lines through the simulation of truncated structures," *IEEE Transactions on Antennas and Propagation*, vol. 59, no. 6, pp. 2188–2195, 2011.